Crossref
DOI: **DOI**: 10.31643/2028/6445.14
Metallurgy and Metallurgical Engineering

Influence of gas flow parameters on the velocity of bulk materials

[1*]Akhmetova S.S., [1]Kabiyeva G.K., [2]Rakhatova A.B.

[1]Abylkas Saginov Karaganda Technical University, Karaganda, Kazakhstan
[2]Saken Seifullin Kazakh Agro Technical Research University, Astana, Kazakhstan

** Corresponding author email: s.akhmetova@ktu.edu.kz*

Received: *April 18, 2026*
Peer-reviewed: *May 19, 2026*
Accepted: *June 5, 2026*

ABSTRACT
This article examines the flow patterns and kinetics of granular media interacting with ascending and descending gas flows. Bulk material release control is a critical aspect of shaft furnace and hopper operation Experimental studies were conducted on a flat transparent model and a close-up "hot" model using high-speed video recording (SK-16). With an error in the calculated values of the critical speed, amounting from to -30.0 to +28.8%, the main parameters varied within the following limits: specific gravity and viscosity of the gas, respectively, from 11.97 to 1.16 N/m³; from $8{,}9 \cdot 10^{-6}$ to $1.81 \cdot 10^{-5}$Pa · s; diameter, specific gravity and coefficient of internal friction of bulk material from $4{,}0 \cdot 10^{-4}$ to $15.0 \cdot 10^{-3}$m; from 14.3 to 39.2 kN/m³; from 0.55 to 0.95; coefficient taking into account the shape of the particles, from 6.0 to 7.8; outlet diameter from0.01 to 0.06 m; attitude $\frac{d}{R}$ equals $0{,}02 - 0{,}4$. The materials studied were agglomerate, lime, millet, and coke; the gas phases were air, helium, and hydrogen. It was established that the outflow mechanism is staged and determined by the frequency of destruction of dynamically unstable vaults. It was found that gas density is the key factor influencing the outflow rate, while the effect of viscosity is secondary. An analytical relationship was formulated for calculating the critical gas velocity that causes layer suspension. The obtained data make it possible to optimize the design parameters of outlet openings and blast supply modes in metallurgical units.

Keywords: bulk materials, gas flow, movement, speed, gas permeability.

Information about authors:

Akhmetova Sandugash Sovetovna — *Candidate of Technical Sciences, Associate Professor of the Department of Higher Mathematics, Abylkas Saginov Karaganda Technical University, 100027, Ave. Nursultan Nazarbayev, 56, Karaganda, Kazakhstan. E-mail: s.akhmetova@ktu.edu.kz; ORCID ID: https://orcid.org/0009-0003-7848-4463*

Kabiyeva Gulnar Kashkimbaevna — *Lecturer, Department of Higher Mathematics, Abylkas Saginov Karaganda Technical University, 100027, Ave. Nursultan Nazarbayev, 56, Karaganda, Kazakhstan. E-mail: g.kabiyeva@ktu.edu.kz; ORCID ID: https://orcid.org/0009-0003-4069-3569*

Rakhatova Aliya Beibutovna — *Doctoral Student, Saken Seifullin Kazakh Agro Technical Research University, 010011, Astana, Zhenis 62 Ave., Kazakhstan. E-mail: aliya-rahatova@mail.ru; ORCID ID: https://orcid.org/0009-0001-9086-232X*

Introduction

When discharged through a horizontal opening, particles of bulk material move across the layer at uneven speeds, causing it to become loosened. This creates the necessary conditions for intensifying heat exchange processes in the moving material layer.

Storage, transportation, and processing of bulk materials are the most common technological operations.

There are two known points of view on the bulk material model:

Firstly, the bulk material model is considered an isotropic conglomerate of tightly bound particles, and the movement of particles within the bulk of the material is possible only when the acting stresses exceed certain limit values. This representation of the bulk material is a consequence of considering the pressure of the material as the primary cause of its movement and flow through openings. This model is only valid for dispersed materials.

Secondly, the model of bulk material is represented as a set of solid, unchanging particles, the connection between which is carried out by dry friction forces.

Although modern numerical methods, such as coupled computational fluid dynamics and discrete element method (CFD-DEM), allow for detailed modeling of individual granule trajectories and local

gas pressure fields [[1], [2], [3], [4], [5]], they still rely heavily on the accuracy of micro-level boundary conditions (such as normal and tangential recovery coefficients, contact stiffness, and local porosity). Moreover, CFD-DEM models require significant computational power when scaled to the actual dimensions of metallurgical furnaces, and they may not always accurately represent the macroscopic analytical relationships of the vault mechanism.

In contrast to numerical simulations, this study proposes an analytical approach based on the fundamental laws of contact mechanics and the moments of friction forces acting directly on the boundary of a dynamically unstable vault. This allows for the derivation of direct criterion dependencies of macro parameters (mass release velocity, critical hover velocity) without the need for end-to-end discrete modeling of millions of particles, ensuring the invariance of the solution for engineering calculations of large-scale vehicles.

The scientific novelty of the work lies in the following:

1. A new analytical macro-model of the mechanics of the destruction of a dynamically unstable vault over an outlet is developed, based on the balance of moments of dry friction forces and the distributed aerodynamic effect of an oncoming or accompanying gas flow. Unlike existing approaches that only consider the gas influence as a volumetric resistance force to the layer, this work is the first to analytically describe the mechanism of changing the frequency of vault formation through changes in the torque acting on adjacent particles of the vault.

2. For the first time, the invariance of the mechanism of loose material release under the influence of gas in relation to gravitational release has been established and theoretically substantiated: it has been proven that the gas flow does not change the kinematic scheme of motion (staged destruction and formation of vaults), but acts as a regulator of the frequency of this process by pushing or dragging the boundary particles.

3. The physical phenomenon of asymmetry in the influence of gas parameters has been identified: it has been proven that the influence of gas viscosity on the critical release parameters is negligible in the developed turbulent regime, while the gas density and layer porosity nonlinearly determine the conditions for complete stagnation. A universal criterion dependence Eq. (12) has been obtained, which improves the accuracy of predicting the critical counterflow velocity by up to 30-50% compared to standard empirical models.

Experimental part

The destruction of a dynamically unstable vault above the outlet occurs as a result of the rolling of adjacent particles under the influence of the torque of frictional forces. In this case, with an increase in the velocity of the oncoming gas flow, one can expect a decrease in the velocity of the particles' rolling relative to each other, which, in turn, will lead to an increase in the lifetime of this vault, and consequently to a decrease in the mass velocity of the material flow [6]. Considering that the torque causing the rolling of two adjacent particles located on a dynamically unstable vault during gravity discharge is equal to:

$$M_1 = T_1 r_1 - T_2 r_2$$

accepting $r_1 = r_2 = r$, we get

$$M_1 = (T_1 - T_2) r$$

or

$$M_1 = T_1 \left(1 - \frac{T_2}{T_1}\right) r \quad (1)$$

where T_1 and T_2– frictional forces between adjacent particles of bulk material, r_1 and r_2 – particle radii.

When a gas flow from below uniformly impacts a dynamically unstable vault, i.e., its entire surface, an additional force appears F, coinciding in direction with the frictional force between particles, therefore:

$$M_2 = T_1 \left(1 - \frac{T_2 + F}{T_1 + F}\right) r. \quad (2)$$

Because $\frac{T_2+F}{T_1+F} < 1$, then with growth$F$this ratio increases, and the value $1 - \frac{T_2+F}{T_1+F}$ decreases. As a result, the torque, the speed of rolling of the material particles, the frequency of destruction (formation) of dynamically unstable arches and, consequently, the rate of flow of the material decrease [7]. The reduction in the rate of flow of the material is also facilitated by the braking of the particles falling out of the arch by the oncoming gas flow. Finally, upon reaching a certain gas velocity, when the ratio $\frac{T_2+F}{T_1+F} \to 1$, the magnitude of the torque will be zero and the release of material ceases. This is also facilitated by the gas flow

supporting the material particles forming the surface of the dynamically unstable vault against the material located above, preventing the particles from rolling [8]. In the limit, the effect of a uniform gas flow from below on the surface of the dynamically unstable vault leads to the layer hanging.

In the case of a layer moving with a co-current gas flow, an increase in its speed to a certain value causes a decrease in the ratio $\frac{T_2-F}{T_1-F}$, and consequently, an increase in torque, particle rolling speed, the frequency of destruction (formation) of dynamically unstable arches, and the rate of material flow. The rate of material flow also increases as a result of the aerodynamic effect of the accompanying gas flow on the descending particles.

To study in detail the mechanism of bulk material flow through a horizontal orifice exposed to counter and cocurrent gas flows, experiments were conducted on a flat transparent model measuring 250 mm in length, 50 mm in width, and 5 mm in depth (Fig.1). The thin depth (5 mm) makes the model virtually two-dimensional, simplifying observation and filming of the processes.

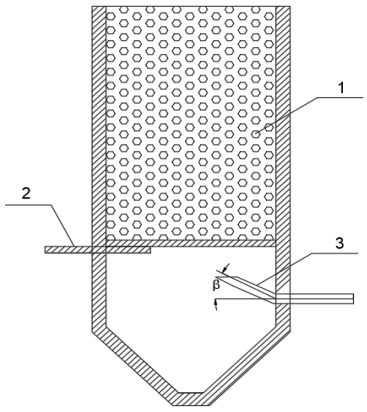

Figure 1 - Scheme of experimental «transparent» model: 1 – charge (шихта); 2 - diaphragm; 3 - nozzle

The experimental procedure involved the following technical specifications:

- Visual Recording: Process dynamics were captured using a high-speed SK-16 motion picture camera. This allowed for a precise frame-by-frame analysis of particle trajectories and the evolution of the dynamically unstable arch formed above the outlet.
- Gas Injection: Gas was introduced into the system in two modes: as a uniform flow exerting pressure on the arch surface, and as concentrated gas jets via specialized nozzles (3) positioned below the outlet [9].
- Flow Measurement: Air flow rates were regulated and monitored using RS-type rotameters, ensuring instantaneous volumetric control with a measurement accuracy of ±3%.
- Experimental Materials: Experiments were conducted using millet, limestone, and agglomerate fractions with particle sizes ranging from 1.45 to 2.44 mm. The material layer height was maintained at 200 mm (±3 mm).
- Data Acquisition: The mass flow rate was determined gravimetrically with a precision of ±50 mg, complemented by visual observations of the flow regime transitions.

Initial observations across all material types indicated that at relatively low gas injection velocities through the nozzles specifically when the velocity ratio (V_1 is the speed of gas movement througt the nozzle and V_2 is the gas velocity ay the outler; S_1 is outlet area, S_2 is the cross section on the gas jet upon meeting the surface):

$$\frac{V_1}{V_2} \leq 20 \text{ and } \frac{S_1}{S_2} \geq 0.38,$$

the system maintains a stable discharge pattern governed by the cyclic collapse of the arch structure.

Here V_1 – the speed of gas movement through the nozzle, V_2 – the gas velocity at the outlet, upon reaching which the material hangs above the outlet, S_1 – outlet area, S_2 – the cross-section of the gas jet upon meeting the surface of a dynamically unstable structure.

As a result of reviewing the filming materials, it was established that as the gas velocity is exceeded, the speed of rolling of the material particles relative to each other decreases, as well as a decrease in the mass velocity of the outflow through the outlet [10].

The mechanism of bulk material flow, both in counter- and co-current gas flows, across the entire studied range of pressure and gas velocity changes, corresponds to gravity release and proceeds through stages of destruction and formation of dynamically unstable vaults. The analysis revealed a dependence of the frequency of destruction (formation) of dynamically unstable vaults on the direction and velocity of the gas flow (Table 1).

Visual observations confirmed that the mechanism of outflow, both in the opposite and in the following flows, retains its staged nature (destruction/formation of arches).

Table 1 -Mechanism of bulk material flow

Flow mode	Frequency of vault failure	Expiration rate	System status
Gravitational	Basic	Standard	Stable
Counter (↑)	It's decreasing	Falls	Risk of hangs
Passing (↓)	It's growing	It's growing	Intensive

It was found that as the counterflow velocity increases, a critical point is reached where the frequency of arch failure becomes minimal, leading to a complete halt of the process. The outflow velocity in the coflow was higher than in the counterflow across the entire pressure range, confirming theoretical calculations on the contribution of aerodynamic forces to particle roll dynamics [11].

To ensure the scalability of laboratory data to industrial processes, fundamental modeling laws were strictly observed [[12], [13]]. To eliminate wall effects and ensure stable granular flow, the following geometric ratios were maintained:

-The ratio of the model shaft diameter to the equivalent particle diameter was >20

-The ratio of the outlet diameter to the particle diameter was >5.

-The ratio of the bed height to the shaft diameter was maintained at ≥ 2

Discussion of the results

Experiments were performed across a wide range of geometric variations, with the outlet-to-shaft diameter ratio ranging from 0.1 to 0.7. The gas flow dynamics, characterized by the Reynolds criterion, included regimes corresponding to the self-similar region. The investigations utilized both «cold» and «hot» laboratory models (Fig. 2 and 3). In the «cold» model, a replaceable diaphragm at the shaft base allowed for outlet diameter variations from 10 to 60 mm. The shaft was mounted on a sealed receiving bin (height: 800 mm, diameter: 250 mm). Gas, with properties detailed in Table 2, was supplied to the system at flow rates up to 60 m³/h via three symmetrically distributed pipes (8 mm diameter) to ensure uniform pressure distribution. The gas supply system was designed to ensure uniform pressure distribution across the material bed. Pipes for gas injection were evenly spaced around the circumference in a horizontal plane, located at distances of 150 mm below and 30 mm above the discharge orifice. In co-current flow experiments (gas and material moving in the same direction), gas was introduced through a sealed plug at the top of the shaft, with subsequent discharge through the receiving hopper [14]. To monitor system pressure, measurement points were flush-mounted with the internal walls of the shaft and hopper. The mass flow rate of the granular medium was recorded with a high precision of ±50 mg.

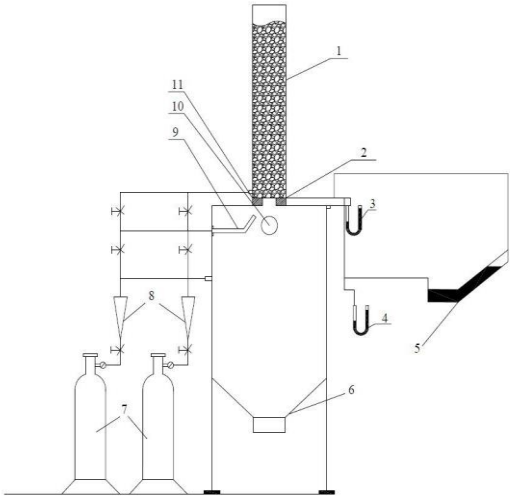

Figure 2 - Model diagram: 1 - shaft; 2 - replaceable diaphragm; 3 and 4 - U-shaped pressure gauges; 5 - micromanometer type MMN; 6 - receiving hopper; 7 - cylinders with compressed gas; 8 - glass rotameters; 9 - gas nozzle; 10 - peephole; 11 - regulating device (damper)

Gas (Table 2), with a flow rate varying within the range of 0 to 60 m³/h, was supplied to the hopper and shaft through three 8 mm diameter pipes, installed evenly around the circumference in the horizontal plane at a distance of 150 mm below and 30 mm above the outlet opening, respectively. When the gas and material moved in the same direction, the gas was supplied through a pipe passed through a plug hermetically sealing the top of the shaft; in this case, the gas was removed from the receiving hopper [[15], [16]]. The ends of the pipes for sampling gas pressure in the receiving hopper and shaft were installed at the level of their walls.

The accuracy of measuring the mass flow rate of bulk material was ± 50 mg.

The «hot» model (Fig. 3) is constructed from individual steel sections lined with fireclay bricks. To ensure a tight seal, the detachable joints are sealed with asbestos gaskets.

Table 2 - Physical properties of the gases used

Gas	Specific gravity, N/m³	Viscosity 10^{-5} Pa· s ·
Hydrogen	1.16	0.89
Helium	1.57	1.95
Air + 62% helium	5.49	1.89
Air + 34% helium	8.44	1.86
Air	11.97	1.81

A lid was attached to the top of the furnace shaft, with steel strip rings welded to the inner surface to divide the gas flow. The cylindrical shaft had an internal diameter of 300 mm, a height of 500 mm, a shoulder height of 200 mm, and a lower diameter of 173 mm. A refractory conical nozzle with the required outlet diameter (60-100 mm) was inserted into the lower part of the shoulders.

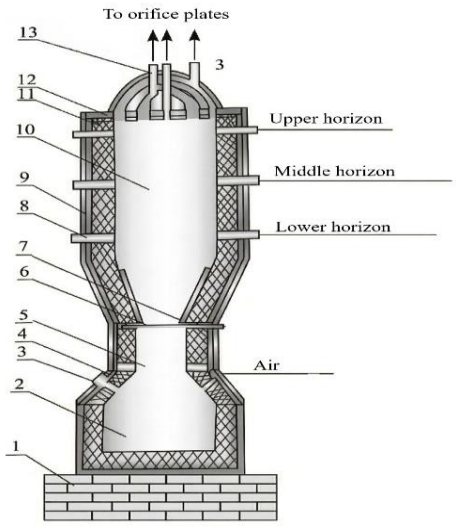

Figure 3 - Schematic diagram of the enlarged model: 1 - foundation; 2 - hearth; 3 - peephole; 4 - hearth dome; 5 - steam; 6 - damper; 7 - refractory cup; 8 - pipes for measuring equipment; 9 - lining; 10 - shaft; 11 - connecting flanges; 12 - gas distribution cover; 13 - pipes for gas outlet

During preparation for and after the experiment, the exhaust port was sealed with a lined damper with holes for gas passage. A hermetically sealed hatch for material release was located in the furnace hearth [17]. The operation of the furnace consists of forced air supply (blast) into the fuel combustion zone to quickly achieve the operating temperature. Air was supplied to the model from the factory line, and hydrogen from cylinders.

Table 3 - Characteristics of bulk materials

Material	Fraction, mm	Equivalent diameter 10^{-3}, m	Coefficient of internal friction
Agglomerate I	3.0 - 10.0	5.48	0.67
Agglomerate II	3.4 - 4.7	4.06	0.67
Agglomerate III	1.6 - 2.5	2.00	0.65
Millet	1.6 - 2.5	2.00	0.55
Limestone I	2.5 - 3.8	3.08	0.57
Limestone II	0.4 - 1.0	0.64	0.56
Coke	1.6 - 2.5	2.00	0.95
Pellets I	5.0 - 15.0	8.66	0.58
Pellets II	4.0 - 6.0	4.90	0.60

The model is equipped with gas flow and pressure control systems using measuring diaphragms, U - shaped pressure gauges and RS type rotameters.

Experiments were conducted on materials with significantly different physical and mechanical properties (Table 3). To determine the mass flow rate of the bulk material, a specific gas flow rate was set and a damper (regulating device) was opened. The material poured into a sealed receiving bin or model forge was weighed, and the mass flow rate was calculated.

Based on the difference in gas pressure below and above the outlet, the pressure drop on the dynamically unstable vault was calculated using the relationship $\Delta P_0 = \Delta P \cdot \frac{d_{eq}}{l_0}$. Where: ΔP is the measured gas pressure drop across the bed; d_{eg} is the equivalent diameter of the material particles; l_0 is the characteristic length (height) of the granular layer.

The freezing of bulk material in the models was determined by a sharp increase in the gas pressure drop and the cessation of pulsations of the working fluid in the pressure gauges, as well as visually through the viewing devices.

Experiments on a «cold» model showed that feeding gas above the outlet and diverting it through the top of the model (Fig. 4, a) has virtually no effect on the material flow rate (Fig. 5, curve a). Feeding gas above the outlet and diverting it through the top of the model and the receiving bin (Fig. 4, b) is more effective, the lower the porosity of the layer in the model. If the material layer has high porosity, then feeding gas has very little effect on the flow rate (Fig. 5, curve b).

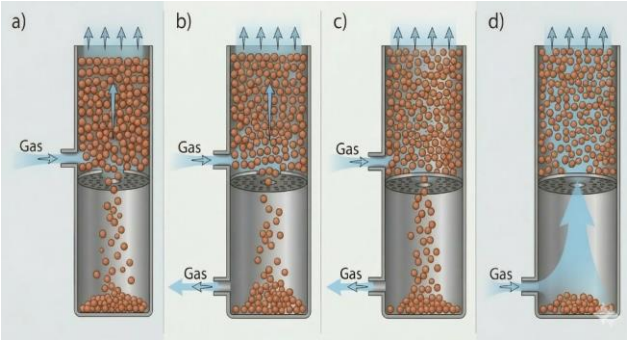

Figure 4- Gas supply diagram for the model: a - gas supply is above the outlet, the top of the model is open, the bottom is closed; b - the same, the top and bottom of the model are open; c - the same, the top of the model is closed, the bottom is open; d - gas supply is below the outlet, the top of the model is open

Reducing the layer's porosity and gas permeability, particularly by replacing the agglomerate layer with millet, results in an increasingly larger portion of the gas flow being directed downward and diverted from the model through the outlet, while the flow rate of the bulk material increases (Fig. 5, curve d). This is explained by the additional downward impact of the gas flow on the descending bulk material in the area of the outlet.

In the case of gas supply to the model above the outlet opening and its removal through the latter (Fig. 4, c), an increase in the gas flow rate or its pressure gradient in the layer in a certain range (Fig. 5, curve c) leads to an increase in the flow rate of bulk materials, which is in good agreement with the results of previously published studies. The lower the gas permeability of the material, the higher its flow rate at a constant gas flow pressure at the inlet (Fig. 6). Changes in the amount of gas supplied to the model, and consequently, its pressure in the bulk material layer, affect the nature of the action of the gas flow passing through a dynamically unstable arch, causing its destruction. In this regard, the conclusion of the authors of the studies about an increase in the flow rate of bulk material with an increase in the pressure gradient in the layer or an equivalent amount of gas supplied to the model becomes clear. The increase in excess pressure above the layer of material increased the additional load from top to bottom on the surface of the dynamically unstable vault, which, in turn, contributed to an increase in the frequency of its destruction, an increase in the initial velocity of movement of particles after the destruction of this vault and an increase in the mass velocity of the outflow of material.

The experimentally recorded dependencies (Fig. 5 and 6) clearly confirm the proposed hypothesis about the mechanism of particle rolling. An increase in the counterflow gas velocity F leads to an asymptotic approach of the moment ratio to unity Eq. (2), which is physically expressed in the stabilization of the dynamic vault and a decrease in its collapse frequency. This refutes the common assumption in simpler empirical models that the release is uniformly slowed down throughout the entire height of the material column, as the key critical resistance is concentrated at the lower boundary of the vault.

From graph 5, it can be seen that the individual series behave differently. Series c and d show a pronounced increase in W_t/W_0 as Q_r/Q_{kr} increases. Series c has the most intense increase, reaching approximately 1.4 at Q_r/Q_{kr} = 4. Series d also increases, but more gradually, reaching a value of approximately 1.2. Series a remains almost unchanged and has a slight downward trend, indicating a slight decrease in W_t/W_0 relative to the initial level. Series b changes slightly and is around 1.0-1.1. Series e decreases sharply when the Q_r/Q_{kr} rises to 1, which indicates a strong difference between this series and the others.

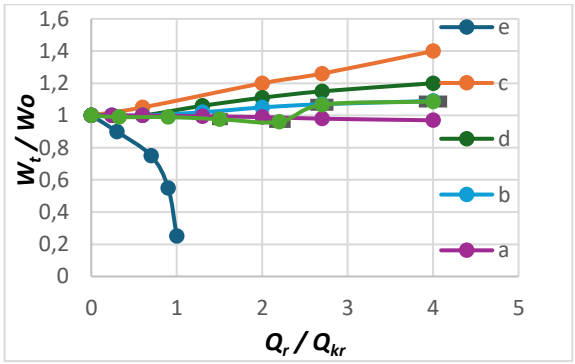

Figure 5 - Dependence of the of the mass flow rate ratio (W_t/W_0) on the normalized gas flow rate (Q_r/Q_{kr}) for different gas supply above the outlet with: (*a*) top removal; (*b*) combined removal (high porosity); (*c*) removal through the orifice; (*d*) combined removal (low porosity); (*e*) counter-current flow (gas supply below the outlet)

The middle line shows the overall average change in the indicator. In general, it is around 1.0-1.1, which indicates a moderate change in W_t/W_0. The error limits show the spread of data relative to the average value: the longer the whiskers, the higher the heterogeneity of the results at a given point. An increase in Q_r/Q_{kr} leads to a different change in W_t/W_0 in individual series.

The most noticeable increase is observed for series c and d, while the most significant decrease is

observed for series e. The average line shows the overall trend, and the error limits reflect the variation between the measurement series.

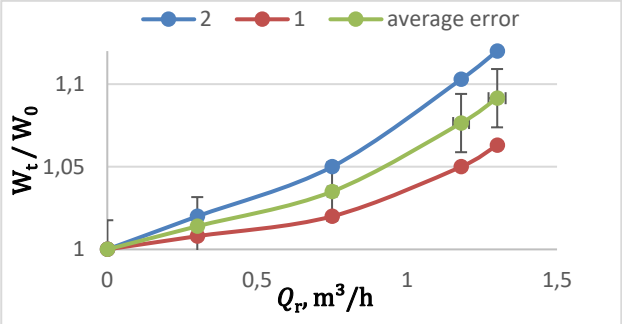

Figure 6 - Dependence of the relative velocity of material flow (W_t/W_0) from the amount of gas (Q_r, m³/h), fed into the model. The diameter of the outlet is 15 mm.
1 - millet; 2 - agglomerate III

The graph 6 shows the dependence of the relative value of W_t/W_0 on the ratio of Q_r.

Lines 1 and 2 represent the minimum and maximum values of the indicator, and the middle line shows the average value. The error limits are plotted on the middle line and show the deviation of the average value from the extreme values.

As Q_r increases from 0 to 1.3, there is a steady increase in the W/W_o value in all data series. This means that there is a direct relationship between the values: the higher the value of Q_r, the higher the relative value of W_t/W_0. For series 1, the W_t/W_0 value increases from 1.000 to 1.063. For series 2, the increase is more pronounced, from 1.000 to 1.120. The average value increases from 1.000 to 1.0915.

It can also be seen that as Q_r increases, the difference between series 1 and 2 increases. At the beginning of the graph, the error is almost non-existent, and at Q_r = 1.3, it reaches its maximum value of ±0.0285. This shows that at higher values of Q_r, the spread of results becomes more noticeable.

Therefore, for the point Q_r = 1.3, the error limit is ±0.0285.

An increase in Q_r leads to an increase in W_t/W_0. At the same time, the average value of W_t/W_0 increases smoothly, and the error value increases as Qr increases, which indicates a greater spread of results at high values of the parameter.

The extreme nature of the dependence of the bulk material flow rate on the amount of air supplied to the model is explained by the change in the distance from the nozzle through which air was supplied to the model to the mouth of the discharge funnel, and consequently to the dynamically unstable arch above the outlet. This distance determines the magnitude of the kinetic energy of the air stream acting on the dynamically unstable arch, which affects the frequency of its destruction (formation) and the rate of material outflow, which is confirmed by the change in the maximum material flow rate depending on the nozzle position [18]. With an increase in the amount of air entering the model, and, accordingly, its velocity, an air channel is apparently formed in the layer of bulk material, passing through the outlet. A decrease in the flow rate of bulk material is explained by the compaction of the material located around the rigid air stream. The probability of the formation of a channel passage of gas is greater, the higher the density of the layer. Naturally, with relatively small dimensions of the outlet opening and high excess air pressure of 9.8 - 29.4 kPa, a complete cessation of material release is expected.

The mass flow rate (G, kg/s) is most often calculated using empirical formulas as the product of the cross-sectional area (S, m²) and the density (ρ, kg/m³) and flow rate (v, m/s), taking into account the flow coefficients: $G=\mu S \rho v$.

Gas outflow:

$$G = C_d \cdot A \cdot \sqrt{2\rho \cdot \Delta P} \qquad (3)$$

where C_d - flow coefficient (empirical); A - hole area; ΔP - pressure drop.

A comparison of the experimental data when gas is supplied to the model according to the scheme shown in Fig. 4 b, c, with the results of calculating the mass flow rate of bulk material using empirical equations shows that the error in the calculated values fluctuates within a fairly wide range: from -25.2 to +47.0%; from -32.5 to +55.6%; from +9.0 to +79.6% respectively. The increased error in the latter case is explained by the different shapes of the outlet openings, which, in our opinion, is consistent with the data from the study.

With increasing gas flow rate supplied below the discharge zone (Fig. 4, d), the flow rate of various bulk materials gradually decreases to 60 – 20% relative to the mass flow rate corresponding to gravity discharge. With a further increase in gas flow rate, the material discharge ceases (Fig. 5, curve d). The wide range of the lower limit of flow rate regulation is explained by the significant differences in the physical and mechanical properties of the bulk materials studied, primarily in particle size distribution, electrical properties, moisture content, adhesion, etc.

A comparison of experimental data with the results of calculating the mass flow rate of bulk materials using empirical equations shows that the error in the calculated values varies widely and amounts to: from -21.0 to +176.0%; from -99.0 to -0.6%; from -100.0 to +67.2 %. The average error is about $\pm 40\%$ and increases sharply when the gas velocity in the outlet approaches the critical value at which the bulk material freezes.

Supplying a certain amount of gas through a nozzle of a smaller diameter allows for a higher velocity of the gas flow and a relatively local nature of its impact on the bulk material adjacent to the point where the jet enters the layer [19].

The kinetic energy of a gas flow acting on the surface of a dynamically unstable vault alters the conditions of its collapse and, consequently, determines the rate of material flow. Therefore, a dependence of the material flow rate on the gas flow parameters was expected.

Experiments have shown that decreasing gas density and viscosity significantly increases the flow rate of the material through the outlet (Fig. 7). The effect of gas viscosity on the flow rate of the bulk material can be clearly seen by comparing the effects of countercurrent flows of hydrogen and helium, which, under the experimental conditions, are similar in density but differ greatly in viscosity (Table 1). Figure 7 shows that the effect of gas viscosity is insignificant, and changes in the flow rate of the material are determined by the density of the gas flow.

Figure 7 shows the dependence of the values of three measurement series and the average error on the speed (V_0), m/s. As the speed increases, there is a general decrease in all the values, but the pattern of decrease varies for each series. The first series shows the most pronounced decrease: at (V_0 = 0), the value is 1, but at (V_0 = 4.9), it decreases to 0.05; at (V_0 = 6.3), the value almost reaches zero. The second row decreases more smoothly: from 1 at the initial speed value to 0.21 at (V_0 = 8.4). The third row is characterized by the most stable decrease: its values remain relatively high for most of the interval and decrease to 0.20 only at (V_0 = 10.4).

The average error also has a downward trend. It decreases from 1 to 0.06, indicating a gradual decrease in the average value of the indicator as the speed increases. The most noticeable decrease in the average error is observed after (V_0 = 3.7), when the differences between the individual rows become more pronounced. Overall, the graph shows that an increase in speed (V_0) leads to a decrease in the indicator under consideration, with the first row being the most sensitive to changes in speed and the third row being the most stable.

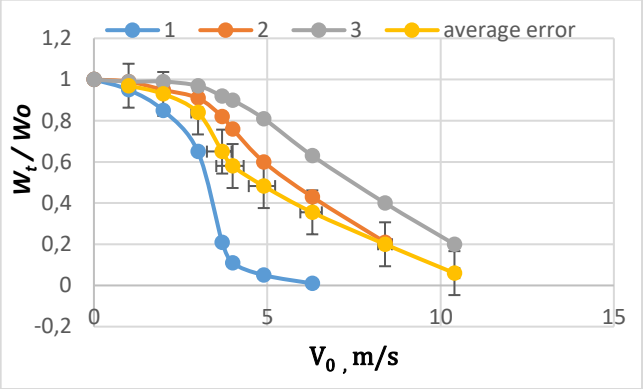

Figure 7 – Dependence of the relative flow rate of agglomerate III (W_t/W_0) from the gas velocity at the outlet (V_0, m/s) with a diameter of 30 mm. 1 - air; 2 - helium; 3 – hydrogen

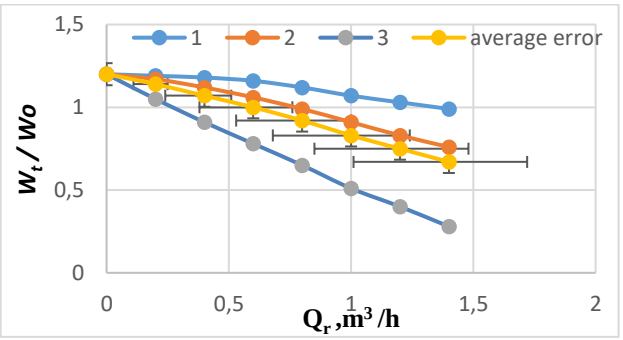

Figure 8 - Dependence of the relative velocity of material flow (W_t/W_0) from its density in air countercurrent (Q_r, m³/h).1 - agglomerate; 2 - limestone; 3 – millet

The fact that in the self-similar (turbulent) region the influence of gas viscosity is leveled out (Fig. 7), indicates the dominance of the inertia forces of the gas jet over the viscous friction forces in the interparticle channels directly at the moment of the vault destruction. This opens up the fundamental possibility of scaling the obtained equations to industrial units working with complex gas mixtures (hydrogen, helium, metallization technological gases) without complicating the calculation algorithms.

When studying the process of controlling the release of a layer in a counter-current gas flow, it was found that the physical properties of the gas do not affect the lower limit of the mass flow rate of the material (Fig. 7). This undoubtedly expands the possibilities for the practical application of methods for controlling the release of bulk materials using a gas flow [20].

The effect of bulk material density on its flow rate is clearly demonstrated in Fig. 8.

Figure 8 shows a graph of the change in the values of three measurement series and the average error. The x-axis shows the argument values from 0 to 1.4 in increments of 0.2, and the y-axis shows the corresponding values of the indicator. All three series show a decreasing trend, but the rate of decrease varies: the first series decreases more smoothly, the second series decreases more pronouncedly, and the third series shows the sharpest decrease. The average error also gradually decreases from 1.20 to 0.67. For the average error line, we have built whiskers that reflect the spread of values between the minimum and maximum values among the three-measurement series at each point. The longer the whiskers, the greater the difference between the individual values. In the initial section, there is almost no spread, as all the values are equal to 1.20. As the argument value increases, the length of the whiskers gradually increases, indicating a growing discrepancy between the measurement series.

It was found that the nature of the material's flow is independent of its physical and mechanical properties. As the size of the material piece used in the experiments increases, the flow rate increases significantly (Fig. 9). Characteristically, as the ratio of the model and outlet diameters decreases, not only does the absolute flow rate of the layer increase, but its lower limit decreases to a certain value at equal gas flow rates, i.e., it becomes possible to control the material release over a wider range.

Figure 9 shows the dependence of two series of values and the average error on the flow rate (Q_r), m³/h. Both series have a decreasing trend, but the rate of decrease differs. The first series decreases smoothly, from 1 at (Q_r = 0) to 0.80 at (Q_r = 12) m³/h. The second series decreases much faster, from 1 to 0 at (Q_r = 8.8) m³/h, indicating a higher sensitivity to changes in flow rate.

The average error also decreases consistently: from 1 to 0.43. The whiskers on the graph reflect the spread between the minimum and maximum values of the two series at each point. At the beginning of the interval, there is no spread because the values of the series are the same. Then, the length of the whiskers gradually increases, indicating an increase in the differences between the first and second series as (Q_r) increases.

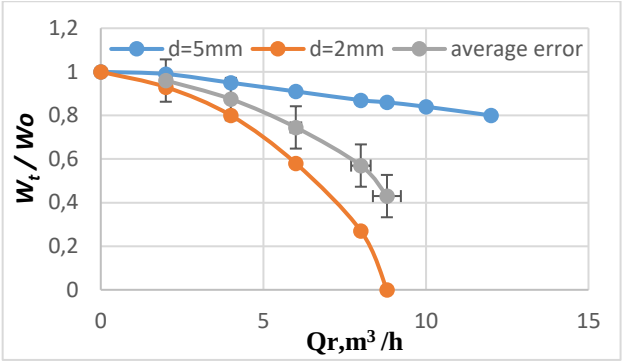

Figure 9 - Dependence of the relative velocity of pellet outflow (W_t/W_0) from the size of the piece (d_{eq}, mm) with air counterflow (Q_r, m³/h).

The physical mechanism of the influence of oncoming and associated gas flows on the kinetics of the outflow, recorded using high-speed video filming SK-16, has a pronounced stage character and is determined by the frequency of destruction of dynamically unstable arches. The observed change in the relative exhaust velocity (W_t/W_0) is due to the redistribution of stress chains inside the dense layer above the outlet (Fig. 8 and 9). The oncoming gas flow passing through the interparticle channels creates an upward aerodynamic pressure, which increases the normal compressive forces between the layer elements. This leads to an increase in the forces of interparticle friction and, as a result, to an increase in the holding torque of the forces acting on the particles in the support nodes of the dynamic vault. The stabilization of the vault blocks the gravitational displacement of the material, causing a decrease in flow rate up to complete stagnation. On the contrary, the oncoming flow reduces the apparent adhesion of the particles, reducing the critical radius of vault formation, which intensifies the release of material due to an increase in the frequency of vault pulsations. The extremum identified in Figure 9 (maximum velocity at d_{eq}=2.0÷2.5 mm) reflects the bifurcation point, where the geometric factor of jamming of large pieces is balanced by the optimal aerodynamic transparency of the pore channels for fluid filtration.

Mathematical analysis of the experimental data allowed for the ranking of investigated parameters based on their influence on the material discharge rate. Under standard conditions, the factors are arranged in the following descending order of significance:

1. Direction of the gas flow;
2. Diameter of the discharge orifice;
3. Bulk density of the granular material;
4. Gas flow rate;

5. Physical properties of the gas (density and viscosity).

Notably, this hierarchy can shift under specific dynamic conditions. For instance, a 30% increase in the gas flow rate causes this parameter to exert a more dominant influence on the discharge rate than the intrinsic bulk density of the material.

To consolidate the experimental findings for both counter-current and co-current gas flow regimes, a unified empirical equation was developed):

$$W_0 = 0.05\gamma_n \frac{D_0^{2.5}}{\sqrt{d_{eq}}} \sqrt{1 \pm \frac{\Delta P}{0.6\gamma_n D_0}} \quad (4)$$

The error associated with this generalized model ranges from **−**19.8% to +23.1%**,** which is significantly lower than the deviations observed when using classical empirical equations. As previously noted, traditional models exhibit errors ranging from −25.1% to +176.1%**,** especially near critical regimes. This confirms that the proposed Eq. (9), which explicitly accounts for the gas-dynamic pressure drop ΔP and orifice geometry rate (D_0) provides a much more reliable tool for industrial design. Comparing the experimental results with calculations of the material mass flow rate under pressure discharge using empirical equations shows that the error in the calculated values varies within a wide range, namely: from −25.1% to +47.1%, from −32.6% to +55.5%, and from +9.8% to +79.5%, respectively.

The limitations of conventional empirical models become even more apparent under counter-current gas flow conditions. For such regimes, the error in mass flow rate calculations using standard equations escalates significantly, with deviations ranging from −21.1% to +176.1%, −99.1% to −0.7%, and −100.0% to +67.1%. On average, the predictive error is approximately ±50%. Notably, this discrepancy increases sharply when transitioning from air typically used in the baseline experiments of previous authors to gases with significantly different physical properties, such as hydrogen or helium (as detailed in Table 1). Such high levels of uncertainty underscore that purely empirical correlations, which do not account for the internal structural mechanics of the granular bed, are unsuitable for complex gas-solid systems. Consequently, there is a clear necessity for a more rigorous theoretical description of the discharge process. By integrating the results of this experimental study with the proposed torque-balance mechanism, it becomes possible to establish a physically consistent model that remains accurate across a wide range of gas-dynamic and material conditions

$$W_0 = \frac{1}{2}\sqrt{2g\mu\left[R + d\left(\frac{1}{2} + \frac{1-\mu}{\sqrt{1+\mu^2}}\right)\right]\left[1 \pm \frac{\Delta P_0}{d\gamma_k f\left(\mu;\frac{d}{R}\right)}\right]} \quad (5)$$

by the area of the outlet opening and the bulk density of the material, we find the mass velocity of its outflow:

$$W_0 = \frac{1}{2}\gamma_n \frac{\bar{n}D_0^2}{4}\sqrt{2g\mu\left[R + d\left(\frac{1}{2} + \frac{1-\mu}{\sqrt{1+\mu^2}}\right)\right]\left[1 \pm \frac{\Delta P_0}{d\gamma_k f(\mu;\frac{d}{R})}\right]} \quad (6)$$

Comparison of experimental data with the results of calculations using dependence (6) shows that the error in the calculated values is within the range from -28.5 to 28.8%.

A comparison of empirical relationships for the critical velocity of a counter-current gas flow demonstrates the varying roles assigned by researchers not only to gas density and viscosity, but also to bulk material density, particle diameters, and the outlet opening [21]. A consequence of this, apparently, is a sharp increase in the error in calculating critical velocity values when processing experimental data using the aforementioned equations, even in the case of an air counter-current [22]. At the same time, gas flow parameters in shaft metallurgical furnaces, and especially in metallization furnaces, can vary widely.

To determine the critical velocity of the counter-flowing gas, a series of experiments were conducted on a «cold» model. The values of the variables were varied within the following limits: outlet diameter $0{,}035 - 0{,}055$m, equivalent diameter of a piece 0.002-0.006 m, specific gravity of gas from 1.2 to 9.2 N/m³ and apparent specific gravity of the material (from 14.5 to 43.5)· 10^3 N/m³.

Assuming equilibrium between the aerodynamic forces and the resisting forces within the granular structure, the following dimensionless relationship can be defined:

$$V'_{kr} = \frac{1}{0.557\sqrt{\gamma_r}} \quad (7)$$

Further transformation of the experimental data into generalized dimensionless coordinates yields:

$$V''_{kr} = \sqrt{\frac{\gamma_k}{437}} \quad (8)$$

Analysis of the experimental datasets demonstrated an approximately linear dependence between the dimensionless critical velocity and the

equivalent flow cross-sectional area. Consequently, the final empirical expression was expressed:

$$V'''_{kr} = \sqrt{\frac{d_{eq}}{0{,}0048} - 0.4} + 0.5 \qquad (9)$$

It has been established that the outlet diameter does not affect the critical velocity of the gas counterflow. In general, the critical velocity of the gas counterflow takes the form:

$$V_{kr} = 0.087\sqrt{\frac{\gamma_k}{\gamma_r}}\left(\sqrt{\frac{d_{eq}}{0.048} - 0.4} + 0.5\right) \qquad (10)$$

The experiment shows that the error in the calculated values ranges from +16.7 to -35.4% and from -28.4 to +24.9%, respectively. Consequently, equation (9) has satisfactory accuracy and is quite acceptable for practical calculations. The influence of gas parameters, the physical and mechanical properties of the bulk material, and the outlet size on the critical velocity of the oncoming gas flow was further studied using volumetric models with gases and materials, the characteristics of which are presented in Tables 1 and 2.

The dependence of the critical counter-current gas velocity V_{kr} on the gas specific weight γ_r is illustrated in Fig. 10. The experimental data for different materials pellets II (1), agglomerate III (2), and millet (3) show a strong correlation with the values calculated using Eq. (17).

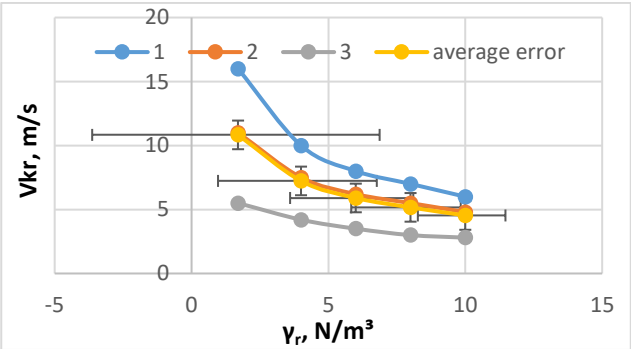

Figure 10 - Dependence of the critical velocity of the counter gas flow (V_{kr}, m/s) from its specific gravity (γ_r, N/m^3). 1 - pellets II; 2 - agglomerate III; 3 - millet; curves - results of calculation according to equation (16)

Figure 10 shows the dependence of three series of values and the average error on the change in the parameter under consideration. All the curves are decreasing, indicating a gradual decrease in the value as the argument increases. The highest values are observed in the first series, which decreases from 16 to 6. The second series also shows a consistent decrease from 11 to 4.8, while the third series has the lowest values and decreases from 5.5 to 2.8.

The average error decreases from 10.83 to 4.533, which confirms the general trend of decreasing the studied indicator. The whiskers on the graph reflect the spread between the minimum and maximum values among the three rows at each point. In the initial section, the spread is the most pronounced, as the difference between the first and third rows is the greatest. As the argument increases, the length of the whiskers gradually decreases, indicating a reduction in the differences between the individual measurement rows.

Thus, the known empirical formulas obtained based on experiments with air flow are valid for calculating the critical gas velocity only within certain limits.

The analytical dependence (5) has been experimentally verified only in the case of air flow. When a loose material is suspended, its flow rate becomes zero when

$$1 - \frac{\Delta P_0}{d\gamma_k f\left(\mu;\frac{d}{R}\right)} = 0 \qquad (11)$$

Revealing the meanings ΔP_0, after substitution and transformations we obtain for the counter gas flow:

$$V_{kr} = m\sqrt{\frac{gd\cdot d_{eq}\gamma_k f\left(\mu;\frac{d}{R}\right)}{2\lambda H\gamma_r}} \qquad (12)$$

Substituting λ and R into equation (12), we obtain

$$V_{kr} = m^{2-n}\sqrt{\frac{g^{1-n}d_{eq}^{1+n}\gamma_k f\left(\mu;\frac{d}{R}\right)}{2cH\gamma_r^{1-n}\eta^n}} \qquad (13)$$

In the case of unstable turbulent motion of the oncoming gas flow ($c = 3.8; n = 0.2$):

$$V_{kr} = m^{1.8}\sqrt{\frac{g^{0.8}d_{eq}^{1.2}\gamma_k f\left(\mu;\frac{d}{R}\right)}{7.6H\gamma_r^{0.8}\eta^{0,2}}} \qquad (14)$$

In turbulent conditions (c=0.55, n=0):

$$V_{kr} = \sqrt{\frac{gd\cdot d_{eq}\gamma_k f\left(\mu;\frac{d}{R}\right)}{1{,}1H\gamma_r}} \qquad (15)$$

Taking $d = d_{eq}$, we obtain for an unstable turbulent regime:

$$V_{kr} = m^{1.8}\sqrt{\frac{g^{0.8}d^{2.2}\gamma_k f\left(\mu;\frac{d}{R}\right)}{7.6H\gamma_r^{0.8}\eta^{0.2}}\cdot\left[\frac{4m}{k(1-m)}\right]^{1.2}} \qquad (16)$$

and for the turbulent regime

$$V_{kr} = md\sqrt{\frac{g\gamma_k f\left(\mu;\frac{d}{R}\right)}{1{,}1H\gamma_r}\cdot\frac{4m}{k(1-m)}} \qquad (17)$$

A comparison of the calculated values of the critical velocities of the counter-current gas flow according to equation (16) and the obtained experimental data showed their satisfactory agreement. The error lies within the range: from -36.4 to +17.1%. Dependence (16) with an accuracy of -25.6 to -35.0% and from -26.3 to -38.4%.

Calculation of critical speeds using formula (16) allows us to reduce the magnitude of the error, which is from -13.9 to +28.8% (Fig. 10) compared with the experimental data. At the same time, the error for the critical velocities of the oncoming air flow, calculated using Eq. (17), is reduced -19.6 to -30.1% and from -18.1 to -32.4% accordingly. This is explained by the significant turbulence of the gas flow in the layer, especially before it freezes.

With an error in the calculated values of the critical speed, amounting from to -30.0 to +28.8%, the main parameters varied within the following limits: specific gravity and viscosity of the gas, respectively, from 11.97 to 1.16 N/m^3; from $8{,}9\cdot 10^{-6}$ to $1.81\cdot 10^{-5}$Pa · s; diameter, specific gravity and coefficient of internal friction of bulk material from $4{,}0\cdot 10^{-4}$ to $15.0\cdot 10^{-3}$m; from 14.3 to 39.2 kN/m^3; from 0.55 to 0.95; coefficient taking into account the shape of the particles, from 6.0 to 7.8; outlet diameter from0.01 to 0.06m; attitude $\frac{d}{R}$ equals $0{,}02-0{,}4$.

A critical finding of this study is the shift in factor significance during the transition to a turbulent counter-current flow. As the system approaches the blockage limit, the influence of gas density increases substantially. Concurrently, the impact of bed porosity, particle size, and shape decreases, while the role of gas viscosity practically disappears. This confirms that at high velocities, the aerodynamic drag acting on the arch structure becomes the primary governing force.

The developed analytical Eq. (12) is universal and demonstrates high accuracy in predicting the critical velocity of counter-current gas flows. It effectively integrates the influence of outlet geometry, solid-phase characteristics, and gas-dynamic parameters. This provides a robust tool for the design and optimization of bulk material flow in horizontal-plane discharge systems, ensuring stable operation in industrial metallurgical furnaces.

Conclusions

Based on the theoretical analysis and a set of experimental studies on "cold" and "hot" models, the following key conclusions were obtained, which constitute the scientific contribution of the work:

1. A physical and mathematical explanation of the mechanism of regulation of the speed of dispersion media by gas flows is proposed, based on the change in the torque of the friction forces during the rolling of particles that form a dynamically unstable vault. It is analytically proven that an oncoming flow minimizes the resulting torque (up to zero at the point of suspension), while a tailing flow maximizes it.

2. The boundaries of applicability of classical empirical release equations have been established, which, as shown in the work, give an error of up to ±50% or more when the gas density and viscosity parameters exceed the normal air conditions. In contrast, the proposed generalized semi-analytical model Eq. (12) stably describes the release kinetics and hover conditions with an error that does not exceed +17.1÷−36.0% in a wide range of changes in the physical and mechanical properties of the phases.

3. The spectrum of factors affecting the controlled release of granular media has been determined and ranked according to their significance: gas velocity vector → hole geometry → bulk density of the material → aerodynamic flow parameters (flow rate, density). It has been revealed that in conditions of developed turbulence, before the layer freezes, the gas density becomes the dominant factor, completely suppressing the influence of the media's viscous characteristics.

4. The practical value of the results lies in the fact that the established macroscopic patterns and criterion equations allow for the precise design of the release and dosing units of hopper systems and counterflow shaft furnaces without conducting expensive and resource-intensive CFD-DEM simulations for each individual particle size.

Conflict of interest. On behalf of all the authors, the correspondingauthor declares that there is no conflict of interest.

CRediT author statement: **S. Akhmetova:** conceptualization, designed the experimental methodology, writing – originaldraft, supervision; **G. Kabiyeva:** methodology and editing; **A. Rakhatova:** writing -review and editing, literature review.

Cite this article as: Akhmetova SS, Kabiyeva GK, Rakhatova AB. Influence of gas flow parameters on the velocity of bulk materials**.** Kompleksnoe Ispolzovanie Mineralnogo Syra = Complex Use of Mineral Resources. 2028; 345(2):29-43. https://doi.org/10.31643/2028/6445.14

Газ ағыны параметрлерінің сусымалы материалдардың ағу жылдамдығына әсері

[1] Ахметова С.С., [2] Кабиева Г.К., [3] Рахатова А.Б.

[1]Ә. Сағынов атындағы Қарағанды техникалық университеті, Қарағанды, Қазақстан
[2]С.Сейфуллин атындағы Қазақ агротехникалық зерттеу университеті, Астана, Қазақстан

Мақала келді: *18 сәуір 2026*
Сараптамадан өтті: *19 мамыр 2026*
Қабылданды: *5 маусым 2026*

ТҮЙІНДЕМЕ

Мақалада жоғары және төмен бағытталған газ ағындарымен өзара әрекеттесу кезінде түйіршікті орталардың ағу заңдылықтары мен қозғалыс кинетикасы зерттеледі. Сусымалы материалдарды тиімді жәшығару процесін басқару шахталық пештер мен бункерлік құрылғыларды пайдалануда маңызды аспект болып табылады. Зерттеулер жазық мөлдір және үлкейтілген «ыстық» модельдерде жылдам бейнетүсірілімді (СК-16) қолдана отырылып жүргізілді. Критикалық жылдамдықтың есептелген мәндеріндегі қателік -30,0-ден +28,8%-ға дейін ауытқыған кезде негізгі параметрлер келесі шектерде өзгерді: газдың меншікті тығыздығы мен тұтқырлығы, тиісінше, 11,97-ден 1,16 Н/м³; $8{,}9\cdot10^{-6}$ бастап $1{,}81\cdot10^{-5}$ Па·с дейін; диаметрі, меншікті тығыздығы және сусымалы материалдың ішкі үйкеліс коэффициенті $4{,}0\cdot10^{-4}$-ден $15{,}0\cdot10^{-3}$ м дейін; 14,3-тен 39,2 кН/м³-ге дейін; 0,55-тен 0,95-ке дейін; бөлшектердің пішінін ескеретін коэффициент, 6,0-ден 7,8-ге дейін; шығыс диаметрі 0,01-ден 0,06 м-ге дейін; d/R қатынасы 0,02-0,4. Зерттелетін материалдар ретінде агломерат, әк, тары және кокс пайдаланылды; газ фазасы ретінде – ауа, гелий және сутегі қолданылды. Ағу механизмі динамикалық тұрақсыз күмбездердің (свод) бұзылу жиілігімен анықталатын сатылы сипатқа ие екені анықталды. Шығару жылдамдылығына әсер ететін негізгі фактор газдың тығыздығы екені, ал тұтқырлықтың әсері екінші дәрежелі екені анықталды. Қабаттың кептелуін (іркілуін) тудыратын газдың критикалық жылдамдығын есептеуге арналған аналитикалық тәуелділік тұжырымдалды. Алынған нәтижелер металлургиялық агрегаттарда шығару тесіктерінің конструктивтік параметрлерін және үрлеу режимдерін оңтайландыруға мүмкіндік береді.

Түйін сөздер: сусымалы материалдар, газ ағыны, қозғалыс, жылдамдық, газөткізгіштік.

Авторлар туралы ақпарат:

Ахметова Сандуғаш Советовна — *Техника ғылымдарының кандидаты, Жоғары математика кафедрасының қауымдастырылған профессоры, Ә. Сағынов атындағы Қарағанды техникалық университеті, 100027, Нұрсұлтан Назарбаев даңғ. 56, Қарағанды, Қазақстан. E-mail: s.akhmetova@ktu.edu.kz; ORCID ID: https://orcid.org/0009-0003-7848-4463*

Кабиева Гульнар Кашкимбаевна — *Жоғарғы математика кафедрасының оқытушысы, Ә. Сағынов атындағы Қарағанды техникалық университеті, 100027, Нұрсұлтан Назарбаев даңғ. 56, Қарағанды, Қазақстан. E-mail: g.kabiyeva@ktu.edu.kz; ORCID ID: https://orcid.org/0009-0003-4069-3569*

Рахатова Алия Бейбутовна — *PHD докторант, Сәкен Сейфуллин атындағы Қазақ агротехникалық зерттеу университеті, 010011, Жеңіс 62 даңғылы, Астана, Қазақстан. E-mail: aliya-rahatova@mail.ru; ORCID ID: https://orcid.org/0009-0001-9086-232X*

Влияние параметров газового потока на скорость истечения сыпучих материалов

[1] Ахметова С.С., [2] Кабиева Г.К., [3] Рахатова А.Б.

[1] Карагандинский технический университет имени А. Сагинова, Караганда, Казахстан
[3] Казахский агротехнический исследовательский университет им. С. Сейфуллина, Астана, Казахстан

Поступила: *18 апреля 2026*
Рецензирование: *19 мая 2026*
Принята в печать: *5 июня 2026*

АННОТАЦИЯ

Статья посвящена исследованию закономерностей истечения и кинетики движения зернистых сред при взаимодействии с восходящими и нисходящими газовыми потоками. Управление выпуском сыпучих материалов является критическим аспектом эксплуатации шахтных печей и бункерных устройств. Экспериментальные исследования проведены на плоской прозрачной и укрупненной «горячей» моделях с использованием скоростной видеосъемки (СК-16). При погрешности в расчетных значениях критической скорости, составляющей от -30,0 до +28,8%, основные параметры изменялись в следующих пределах: удельная плотность и вязкость газа, соответственно, от 11,97 до 1,16 Н/м³; от 8,9 ·

	10^{-6} до $1.81 \cdot 10^{-5}$ Па·с; диаметр, удельная плотность и коэффициент внутреннего трения сыпучего материала от $4{,}0 \cdot 10^{-4}$ до $15{,}0 \cdot 10^{-3}$м; от 14,3 до 39,2 кН/м³; от 0,55 до 0,95; коэффициент, учитывающий форму частиц, от 6,0 до 7,8; диаметр выходного отверстия от 0,01 до 0,06 м; отношение d/R равно 0,02-0,4. В качестве исследуемых материалов использованы агломерат, известь, пшено и кокс; в качестве газовой фазы — воздух, гелий и водород. Установлено, что механизм истечения носит стадийный характер и определяется частотой разрушения динамически неустойчивых сводов. Выявлено, что ключевым фактором, влияющим на скорость выпуска, является плотность газа, в то время как влияние вязкости вторично. Сформулирована аналитическая зависимость для расчета критической скорости газа, вызывающей зависание слоя. Полученные данные позволяют оптимизировать конструктивные параметры выпускных отверстий и режимы подачи дутья в металлургических агрегатах.
	Ключевые слова: сыпучие материалы, газовый поток, движение, скорость, газопроницаемость.
Ахметова Сандугаш Советовна	***Информация об авторах:*** *Кандидат технических наук, ассоциированный профессор кафедры Высшая математика, Карагандинский технический университет им. А.Сагинова, 100027, пр. Нурсултана Назарбаева, 56, Караганда, Казахстан. E-mail: s.akhmetova@ktu.edu.kz; ORCID ID: https://orcid.org/0009-0003-7848-4463*
Кабиева Гульнар Кашкимбаевна	*Преподаватель кафедры Высшая математика, Карагандинский технический университета им. А.Сагинова, 100027, пр. Нурсултана Назарбаева, 56, Караганда, Казахстан. E-mail: g.kabiyeva@ktu.edu.kz; ORCID ID: https://orcid.org/0009-0003-4069-3569*
Рахатова Алия Бейбутовна	*Докторант PHD, Казахский агротехнический исследовательский университет имени Сакена Сейфуллина 010011, пр. Жеңіс, 62, Астана, Казахстан. E-mail: aliya-rahatova@mail.ru; ORCID ID: https://orcid.org/0009-0001-9086-232X*

References

[1] Guo C, Liu G, Wang X. CFD-DEM coupling analysis of EPB screw conveyor muck discharge in water-rich sandy cobble strata // Scientific Reports. 2026; 16(1):12407. https://doi.org/10.1038/s41598-026-41903-7

[2] Xiao F, Luo M, Huang F, et al. CFD–DEM investigation of gas-solid flow and wall erosion of vortex elbows conveying coarse particles. Powder Technology. 2023; 424:118524. https://doi.org/10.1016/j.powtec.2023.118524

[3] Heng Zhou, Kun Xu, Xu Tian, et al. Influence of burden profile on gas-solid distribution in COREX shaft furnace with center gas supply by CFD-DEM model. Powder Technology. 2021; 392:672–679. https://doi.org/10.1016/j.powtec.2021.07.039

[4] Fei Xiao, Min Luo, Fayuan Huang, et al. CFD – DEM investigation of gas-solid flow and wall erosion of vortex elbows conveying coarse particles. Powder Technology. 2023; 424:118524. https://doi.org/10.1016/j.powtec.2023.118524

[5] Banik R K, Das H J. MFIX – DEM simulation of gas-solid flow dynamics in a dual fluidized bed system. IOP Conference Series: Earth and Environmental Science. 2024; 1372(1):012100. https://doi.org/10.1088/1755-1315/1372/1/012100

[6] Maksimov E V, Bekbaev K S, Tarabaev B K, et al. Issledovaniye protsessa porchi sypuchikh materialov v szhatykh usloviyakh [Investigation of the expiration of bulk materials in summary conditions]. Vestnik nauki Kazakhskogo agrotekhnicheskogo universiteta im. S. Seyfullina [Herald of Science of S. Seifullin Kazakh Agrotechnical University]. 2012; 4(75):94–98. (In Russ.).

[7] Mankoc C, Janda A, Arévalo R, et al. The flow rate of granular materials through an orifice. Granular Matter. 2007; 9(6):407–414. https://doi.org/10.1007/s10035-007-0062-2

[8] Amanbaev T R, Antony S J. Modeling the Outflow of Particulate Solids from a Container Taking into Account the Effect of Adhesion to the Wall. 2022; 57:954–966. https://doi.org/10.1134/S0015462822070023

[9] Chen J, Ge M, Li L, Zheng G. Material transport and flow pattern characteristics of gas–liquid–solid mixed flows. Processes. 2023; 11(8):2254. https://doi.org/10.3390/pr11082254

[10] Tingwen Li, Erik Delsman, Sreekanth Pannala. Mass flow rate prediction for gas-controlled hopper discharge of free-flowing granular materials. Powder Technology. 2026; 473:122190. https://doi.org/10.1016/j.powtec.2026.122190

[11] Ferrari G, Poletto M. Arch-Free flow in aerated silo discharge of cohesive powders. Powder Technology. 2009; 191(1-2):118–125. https://doi.org/10.1016/j.powtec.2008.10.013

[12] Zhanxia D, Yan B, Huang M, Cheng B. Numerical simulation of reduction behavior in shaft furnace based on DEM and CFD // International Journal of Chemical Reactor Engineering. – 2025. – Vol. 23, No. 3. – P. 373–391. https://doi.org/10.1515/ijcre-2024-0109

[13] Xu T, Zhou H, Zhang Y, et al. Numerical simulation of hydrogen-enriched shaft furnace. International Journal of Hydrogen Energy. 2024; 55:1131–1142. https://doi.org/10.1016/j.ijhydene.2023.11.277

[14] Zhou H, Xu K, Tian X, et al. Influence of burden profile on gas-solid distribution in COREX shaft furnace with center gas supply by CFD-DEM model. Powder Technology. 2021; 392:672–679. https://doi.org/10.1016/j.powtec.2021.07.039

[15] Wan Q, Zhao Z, Wang R, Tang M, Wang D, Zhang S, Hu B. Characteristics of Gas–Solid Flow in an Intermittent Countercurrent Moving Bed. Processes. 2022; 10(10):2116. https://doi.org/10.3390/pr10102116

[16] Vynnycky M, Rangavittal B V, Glaser B. An Asymptotic Model for Gas-Solid Flow in a Countercurrent Moving Bed Reactor. SIAM Journal on Applied Mathematics. 2023; 83(2):605–631. https://doi.org/10.1137/22M1496293

[17] Chen X, Chen J, Cai C, Liang X. Discharge characteristics of granular coal with wide size distribution from aeration silo. Journal of Chemical Industry and Engineering. China. 2011; 62(6):1654–1661. https://doi.org/10.3969/j.issn.0438-1157.2011.06.031

[18] Chen J, Ge M, Li L, Zheng G. Material transport and flow pattern characteristics of gas–liquid–solid mixed flows. Processes. 2023; 11(8):2254. https://doi.org/10.3390/pr11082254

[19] Li T, Delsman E, Pannala S. Mass flow rate prediction for gas-controlled hopper discharge of free-flowing granular materials. Powder Technology. 2026; 473:122190. https://doi.org/10.1016/j.powtec.2026.122190

[20] Zhu X, Dong P, Tu Q, Zhu Z, Wang H. Investigation of gas–solids flow characteristics in a pressurised circulating fluidised bed by experiment and simulation. Powder Technology. 2020; 366:420–433. https://doi.org/10.1016/j.powtec.2020.02.047

[21] Zhang X, Yu Y, Hu Y. Experimental study on gas–liquid–solid interaction characteristics in the launch tube. Journal of Marine Science and Engineering. 2022; 10(9):1239. https://doi.org/10.3390/jmse10091239

[22] Yang S-C, Hsiau S-S. The simulation and experimental study of granular materials discharged from a silo with the placement of inserts. Powder Technology. 2001; 120(3):244–255. https://doi.org/10.1016/S0032-5910(01)00277-7